Biochimica et Biophysica Acta 1804 (2010) 1817–1831

Contents lists available at ScienceDirect

Biochimica et Biophysica Acta

journal homepage: www.elsevier.com/locate/bbapap

Kinetic and structural characterization of caspase-3 and caspase-8 inhibition by a novel class of irreversible inhibitors

Zhigang Wang [a,*], William Watt [b,1], Nathan A. Brooks [b,2], Melissa S. Harris [c], Jan Urban [d], Douglas Boatman [e], Michael McMillan [f], Michael Kahn [f,g,h], Robert L. Heinrikson [i], Barry C. Finzel [b,3], Arthur J. Wittwer [j], James Blinn [j], Satwik Kamtekar [j,4], Alfredo G. Tomasselli [j,*,5]

[a] Oligonucleotide Therapeutics Unit, Pfizer, Inc., 620 Memorial Drive, Cambridge, MA 02139, USA
[b] Global Research and Development, Pfizer, Inc., 301 Henrietta Street, Kalamazoo, MI 49007, USA
[c] Global Research and Development, Pfizer, Inc., 216 Eastern Pointe Rd, Groton, CT 06840, USA
[d] 8841 Helen James Avenue, San Diego, CA 92126, USA
[e] Arena Pharmaceuticals, 6166 Nancy Ridge Dr., San Diego, CA 92121, USA
[f] Eli and Edythe Broad Center for Regenerative Medicine and Stem Cell Research, University of Southern California, 1501 San Pablo St., Los Angeles, CA 90033, USA
[g] Department of Biochemistry and Molecular Biology, Keck School of Medicine, University of Southern California, 1501 San Pablo St., Los Angeles, CA 90033, USA
[h] Department of Molecular Pharmacology and Toxicology, School of Pharmacy, University of Southern California, 1501 San Pablo St., Los Angeles, CA 90033, USA
[i] Proteos, Inc., 4717 Campus Drive, Kalamazoo, MI 49008, USA
[j] Global Research and Development, Pfizer, Inc., 700 Chesterfield Parkway West, Chesterfield, MO 63017, USA

ARTICLE INFO

Article history:
Received 29 January 2010
Received in revised form 1 May 2010
Accepted 17 May 2010
Available online 24 May 2010

Keywords:
Caspase-3
Caspase-8
Peptidomimetic inhibitors
Irreversible inhibition
Urazole
Crystal structure

ABSTRACT

Because of their central role in programmed cell death, the caspases are attractive targets for developing new therapeutics against cancer and autoimmunity, myocardial infarction and ischemic damage, and neurodegenerative diseases. We chose to target caspase-3, an executioner caspase, and caspase-8, an initiator caspase, based on the vast amount of information linking their functions to diseases. Through a structure-based drug design approach, a number of novel β-strand peptidomimetic compounds were synthesized. Kinetic studies of caspase-3 and caspase-8 inhibition were carried out with these urazole ring-containing irreversible peptidomimetics and a known irreversible caspase inhibitor, Z-VAD-fmk. Using a stopped-flow fluorescence assay, we were able to determine individual kinetic parameters of caspase-3 and caspase-8 inhibition by these inhibitors. Z-VAD-fmk and the peptidomimetic inhibitors inhibit caspase-3 and caspase-8 via a three-step kinetic mechanism. Inhibition of both caspase-3 and caspase-8 by Z-VAD-fmk and of caspase-3 by the peptidomimetic inhibitors proceeds via two rapid equilibrium steps followed by a relatively fast inactivation step. However, caspase-8 inhibition by the peptidomimetics goes through a rapid equilibrium step, a slow-binding reversible step, and an extremely slow inactivation step. The crystal structures of inhibitor complexes of caspases-3 and -8 validate the design of the inhibitors by illustrating in detail how they mimic peptide substrates. One of the caspase-8 structures also shows binding at a secondary, allosteric site, providing a possible route to the development of noncovalent small molecule modulators of caspase activity.

1. Introduction

Apoptosis, or programmed cell death [1], is an essential biological process occurring in cells as a component of animal development, tissue homeostasis, and immune responses [2–4]. Although the apoptotic process is a normal and essential physiological event in healthy organisms, in pathological states, it can be abrogated as in cancer [5] and autoimmunity [6], or exacerbated as in stroke [7], neurodegeneration [8], retinal cell death [9], myocardial and liver ischemia [10,11], and inflammatory diseases such as sepsis [12], osteoarthritis [13], rheumatoid arthritis [14], and asthma [15]. Promoting apoptosis in cancer [16] or attenuating it in stroke, neurodegeneration, and inflammation [17–19] may be viable

Abbreviations: AMC, 7-amino-4-methyl-coumarin; DMSO, dimethyl sulfoxide; DTT, dithiothreitol; fmk, flouromethyl ketone; MMX, Molecumetics Company, Ltd; RMSD, root mean squared deviation

* Corresponding authors.
E-mail addresses: zhigang.wang@pfizer.com (Z. Wang), atomasse@gmail.com (A.G. Tomasselli).
[1] Present address: 7262 Atlantic Ave., South Haven, MI 49090, USA.
[2] Present address: Lilly Research Laboratories, Eli Lilly and Co., Indianapolis, Indiana 46285, USA.
[3] Present address: Medicinal Chemistry Department, College of Pharmacy, University of Minnesota, 308 Harvard St., S.E., Minneapolis, MN 55455, USA.
[4] Present address: Pacific Biosciences, 1505 Adams Drive, Menlo Park, CA 94025, USA.
[5] Present address: 1540 Garden Valley, Wildwood, MO 63038, USA.

1570-9639/$ – see front matter © 2010 Published by Elsevier B.V.
doi:10.1016/j.bbapap.2010.05.007

approaches to treat these devastating diseases, most of which continue to defy therapeutic intervention.

Caspases, a family of related cysteinyl proteinases, mediate critical steps of the apoptotic process [20–23]. These enzymes are exquisitely specific molecular scissors that employ the cysteinyl thiol group as a nucleophile to catalyze the cleavage of peptide bonds having an aspartic acid at the P_1 position. Fourteen caspases have been reported to date and human orthologs have been identified for twelve of these [24]. Caspases have been classified with respect to their functions into three categories: (a) initiator caspases, (b) executioner caspases, and (c) inflammatory or cytokine processing caspases. All caspases are synthesized in cells as inactive zymogens that contain a prosegment, a large N-terminal, and a smaller C-terminal segment that are processed during enzyme activation to produce the A and B chains, respectively, of the caspase heterodimer. The prosegment, large in the initiator caspases and short in the executioner caspases, appears to direct the course of activation and determine the location of the proenzyme in the cell. The initiator procaspase-8 participates in the extrinsic pathway that is set in motion by ligand-induced activation of the death receptor at the plasma membrane and proceeds with procaspase-8 recruitment. These events foster procaspase-8 dimerization and activation in a mechanism independent of intersubunit cleavage [22,25,26]. Another apoptotic pathway involving an initiator caspase is the intrinsic pathway that is triggered by an insult to the cell, e.g., to the mitochondria, leading to the release of cytochrome *c* with the subsequent formation of a complex consisting of Apaf-1, procaspase-9, and cytochrome *c*. This results in procaspase-9 activation and is also independent of intersubunit cleavage [27]. In both pathways, the activated initiator caspases transduce the apoptotic signal by proteolytically processing and activating the downstream executioner procaspases, caspase-3, -6, and -7. The executioner procaspases are constitutive dimers, and cleavage of the intersubunit linkers by initiator caspases allows the formation of catalytically competent enzyme heterodimers [22,26]. These, in turn, lead to the degradation of cell cycle proteins, DNA repair enzymes, and cytoskeleton proteins in the apoptotic process of programmed cell death. The inflammatory procaspases undergo an activation process similar to that of initiator procaspases to acquire the catalytic activity for cytokine processing [25].

An enormous body of information has been generated for caspases, and the X-ray structures of caspase-1 [28,29], caspase-2 [30], caspase-3 [31–34], caspase-6 [35], caspase-7 [36,37], caspase-8 [38–40], and caspase-9 [41] have been determined.

Intense efforts during the past 15 years to find drugs that inhibit caspases have produced several clinical candidates, but no caspase inhibitor has yet reached the market [17–19]. Because these enzymes have shallow and widely dispersed active sites, it has been necessary to design chemically reactive compounds to achieve potent inhibition of enzyme activity. Generally speaking, caspase inhibitors are composed of three parts: an active site recognition element, the P_1 aspartic acid to confer caspase specificity, and a reactive electrophilic warhead that is capable of forming a covalent linkage (reversible or irreversible) with the nucleophilic active site thiol of the enzyme. Electrophilic warheads include aldehydes, chloromethyl ketones [42], epoxides [43], and vinyl sulphones [44], all of which react readily with thiols. To deliver these warheads selectively to the thiol in the target of interest, it is necessary to build in a recognition element that will concentrate the inhibitor at the active site of the target. Many inhibitor design strategies have been used to devise recognition elements mostly by changing the P_1–P_3 amino acids in a tetrapeptide of the natural caspase substrates with a myriad of different chemical moieties. These efforts have resulted in the generation of inhibitors with various degrees of peptidic features. Addition of warheads to such peptide-based inhibitors of caspases has produced molecules that were efficacious when tested in animal models representative of various human diseases: they include liver diseases, traumatic brain injury, myocardial infarction, and stroke [17–19]. Pralnacasan (VX-740), an inhibitor of caspase-1, reached clinical Phase II for rheumatoid arthritis and osteoarthritis but was subsequently discontinued due to liver problems with its prolonged use. VX-765 has completed Phase IIa studies for psoriasis, but results have not been reported [17,18]. IDN-6556, a peptidomimetic irreversible inhibitor of caspase-1, -3, -6,-7,-8, and -9, was very effective in rodent model of liver diseases and has reached Phase II in trials for patients with chronic hepatitis C and trials for patients undergoing liver transplantation [17,18].

Development of nonpeptide inhibitors is being pursued by various pharmaceutical companies to circumvent poor membrane penetration, short half-life in vivo, and other undesirable pharmacokinetic properties characteristic of peptide-based inhibitors [17–19]. For most proteases, substrates and peptidomimetic inhibitors adopt a β-strand conformation, and such is the case for the caspases [32,38]. The recognition element for a caspase inhibitor, therefore, might mimic a β-strand and include an aspartic acid or mimic thereof at the P_1 position. In a search for nonpeptide chemical scaffolds that mimic peptide secondary structures, Kim and Kahn [45] used solid-phase organic synthesis to construct bicyclic templates reflecting an extended β-strand conformation. This approach was previously validated with the design, synthesis, and evaluation of serine proteinase thrombin inhibitors with K_I values in the subnanomolar range [46,47]. We have investigated an alternate β-strand peptidomimetic scaffold of Kim and Kahn [45] incorporating a urazolopyridazine template for structure-based design of caspase inhibitors. Both types of inhibitors block the enzyme by forming a thiohemiketal complex, but the irreversible inhibitors have a leaving group, 2,5-dichlorobenzoate, and inactivate the enzyme permanently through its expulsion (Scheme 1).

Here we report kinetic studies and structural characterization of caspase-3 and caspase-8 inhibition by these novel β-strand irreversible peptidomimetic inhibitors (hereafter referred to as Compound-1, -2, -3, -4, -5, -6, -7, -8, and -9, or "MMX" inhibitors), and by Z-VAD-fmk, a widely used irreversible caspase inhibitor. The executioner caspase-3 and initiator caspase-8 were chosen because they have similar active sites and common processing patterns of activation, yet operate at distinct points in the apoptotic cascade. Using a stopped-flow fluorescence assay, we were able to determine the individual kinetic parameters of caspase-3 and caspase-8 inhibition by Z-VAD-fmk and a number of irreversible peptidomimetic inhibitors. Structures of three complexes of caspase-3 and caspase-8 with these novel peptidomimetic inhibitors have been solved to high resolution. The kinetic and structural results are discussed in light of the subtle difference between the two caspases and their inhibition mechanisms.

2. Materials and methods

Active and highly pure recombinant, human caspase-3 and caspase-8 were obtained as previously described [48,49], although in the present work, we have used the wild type sequence of caspase-3 containing Asp^{190} and Trp^{206} instead of to Glu^{190} and Arg^{206} previously used [48]. Upon purification and activation, caspase-3 subunits A and B were processed to yield the sequences S^{29}GIS…IETD^{175} and S^{176}GVD…YFYH^{277}-$(H)_7$, respectively (nomenclature of Rank et al. [48]). On the other hand, the caspase-8 sequence is the one expressed earlier [49]; upon refolding and purification, mature caspase-8 yielded the sequences S^{18}PRE…VETD^{181} and L^{192}SSP…FPSD^{286}, for subunits A and B, respectively (nomenclature of Koeplinger et al. [49]). Purified caspase-3 and purified and refolded caspase-8 were about 90% and 85% active, respectively by active site titration. Caspase substrates, Ac-DEVD-AMC and Ac-IETD-AMC, were purchased from Peptide Institute, Inc. Z-VAD-fmk was purchased from Bachem Bioscience, Inc. Substrates and inhibitors are dissolved

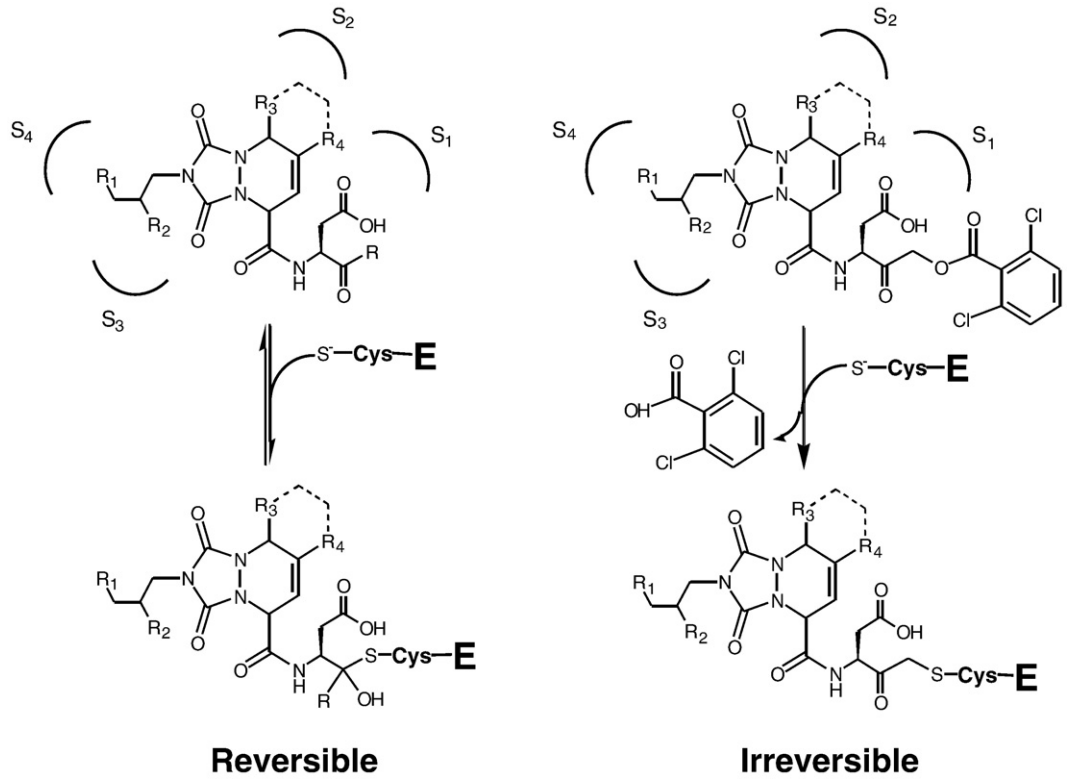

Scheme 1. β-strand peptidomimetic scaffold incorporating a urazolopyridazine template for structure-based design of caspase reversible and irreversible inhibitors.

in DMSO to make concentrated stock solutions. DTT-containing buffers were made fresh every day by dissolving DTT in buffer stocks without readjusting the pH. The buffers were then degassed and used to dilute either the enzyme or substrate and inhibitor. All other reagents were of the highest purity available from commercial sources.

2.1. Synthesis of inhibitors

Scheme 2 provides a representation of inhibitor synthesis following the procedures described in earlier works [50,51]. Isobutylchloroformate (5.0 ml, 39 mmol) was added to a solution of *N*-Fmoc-(*O*-*t*-Bu)-aspartic acid (14.5 g, 35.2 mmol) stirred in THF (350 ml) in a flask cooled to −25 °C and followed by *N*-methylmorpholine (4.3 ml 39 mmol). The resulting mixture was stirred for 10 min, and then a solution of diazomethane in diethyl ether (140 ml, ca. 1 mmol/ml) was added. The solution was kept stirring in the cold bath for 1 h, then allowed to warm to room temperature and stirred an additional 1.5 h. The solution was diluted with ethyl acetate and washed with saturated aqueous $NaHCO_3$ solution, water, and saturated aqueous NaCl solution. The organic solution was dried over anhydrous sodium sulfate, filtered, and concentrated under vacuum to a pale yellow foam. The foam was dissolved in THF (250 ml) and the flask was immersed in a dry ice/acetone bath. Hydrogen bromide (4.6 ml, 48% aqueous) was added slowly and the solution was stirred for 30 min. in the dry ice/acetone bath, then for 1.5 h in an ice/water bath. The solution was concentrated on a rotary evaporator to ca. 100 ml then diluted with ethyl acetate and washed with saturated aqueous $NaHCO_3$ solution, water and saturated aqueous NaCl solution. The organic layer was dried over anhydrous magnesium sulfate, filtered, and concentrated under vacuum to give 20.6 g of the product as a pale viscous oil. The crude product was dissolved in DMF (375 ml), and 2,6-dichlorobenzoic acid was added followed by solid $NaHCO_3$ (4.23 g, 50.4 mmol) and potassium iodide (7.66 g, 46.1 mmol). The mixture was stirred under an anhydrous nitrogen atmosphere for 16 h then concentrated under vacuum. The residue was dissolved in ethyl acetate and washed with saturated aqueous $NaHCO_3$ and brine, then dried over anhydrous magnesium sulfate, filtered, and concentrated under vacuum to a brown oil. The oil was purified by flash chromatography to give 21 g (96% yield) of the product as an off-white solid. The solid was dissolved in 400 ml of 1:1 TFA/methylene chloride and the solution was stirred for 3.5 h at ambient temperature then concentrated under vacuum to 19.1 g of an off-white solid. This product was used in subsequent steps without further purification.

2-Chlorotrityl chloride resin (3.7 g, 1.33 mmol/g) was shaken with a solution of 5 ml of thionyl chloride in 95 ml of methylene chloride for 30 min. The resin was filtered then washed with methylene chloride (5×50 ml). The resin was taken up in methylene chloride (40 ml), then the acid was added followed by diisopropylethylamine and the mixture was shaken for 2.5 h. Methanol (10 ml) and diisopropylethylamine were added, and shaking was continued for 30 min. The resin was filtered and washed with dimethylformamide (5×30 ml), methylene chloride (5×30 ml), and diethyl ether (3×30 ml) then dried in a vacuum desiccator. Fmoc analysis indicated 0.33 mmol/g attached amino acid. The resin was taken up in a mixture of tetrahydrofuran, methylene chloride, and methanol (5:4:1, 40 ml), and sodium borohydride was added with vigorous gas evolution. The mixture was shaken for 45 min then filtered, and the resin was washed with DMF (5×20 ml), methanol (3×20 ml), and methylene chloride (3×20 ml). The resin was shaken with 25% piperidine in DMF (20 ml) for 5 min. then filtered and treated for another 5 min with 25% piperidine in DMF. The resin was filtered and washed with DMF (5×20 ml), methylene chloride (5×20 ml), and diethyl ether (3×20 ml) then dried in a vacuum desiccator.

The resin was divided into portions (50 mg, ca. 0.22 mmol), and the appropriate dienoic acid (0.6 mmol) was added. The mixture was then treated with a solution of 0.6 M PyBOP, 0.6 M HOBt, and 1.2 M diisopropylethylamine in DMF (1 ml). The mixture was shaken until Kaiser analysis of a resin sample indicated complete conversion of the amine (1 h) when the resins were rinsed with DMF (3×1 ml) and

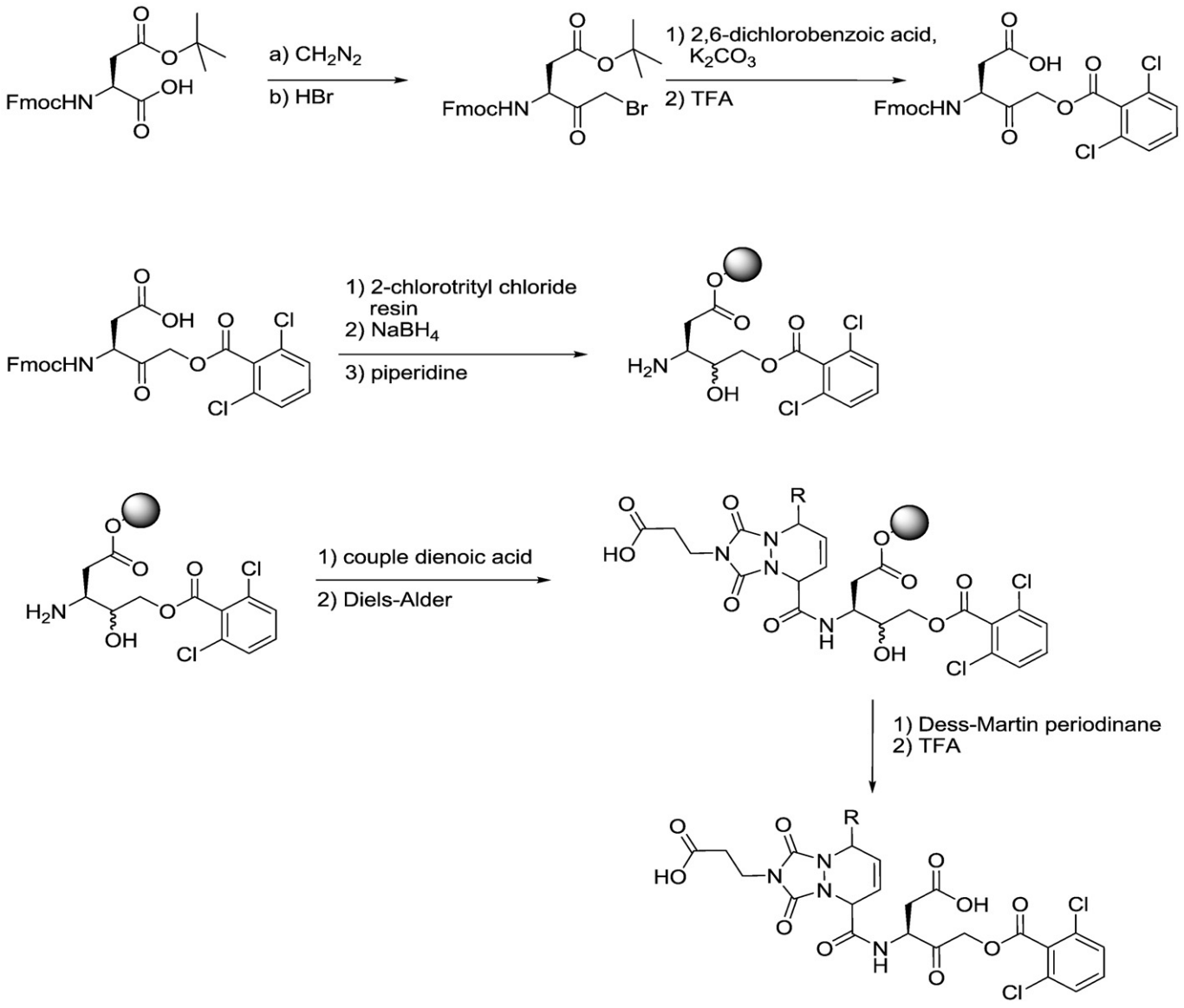

Scheme 2. Representation of inhibitor synthesis.

methylene chloride (3 × 1 ml). Each resin was treated with 1 ml of a freshly prepared solution resulting from combining the appropriate urazole (0.5 mmol) with bis(trifluoroacetoxy)iodobenzene (0.5 mmol) in DMF (10 ml). These mixtures were shaken for 1 h, then the resins were washed with DMF (4 × 1 ml) and methylene chloride (3 × 1 ml). The resins were then treated with 1 ml of a 0.7 M solution of Dess–Martin periodinane in methylene chloride and DMSO (1:1) for 3 h. The resins were filtered and washed with DMF (4 × 1 ml) and methylene chloride (3 × 1 ml). Each resin was treated for 30 min with 1 ml of 95% TFA/methylene chloride (3:1) and then washed twice with 95% TFA/methylene chloride. The combined filtrates were concentrated under vacuum then the residue was dissolved in acetic acid and lyophilized to give the product as a powder. All inhibitors employed in the present study were >95% pure as judged by HPLC/MS.

2.2. Stopped-flow kinetic experiments

All kinetic experiments were carried out on a Hi-Tech SF-61DX2 stopped-flow system in 100 mM $NaPO_4$/10 mM Tris–HCl buffer containing 0.001% Tween-20, 2% DMSO, and 50 mM DTT at pH 7.5 (for caspase-3) and pH 7.2 (for caspase-8) at 25 °C. Ac-DEVD-AMC and Ac-IETD-AMC were employed as substrates of caspase-3 and caspase-8, respectively. Upon cleavage, both substrates released the fluorescent AMC, which was then measured by its fluorescence emission at 450 nm. Fluorescence measurements employed an excitation wavelength that was set at 350 nm with a monochromator, and the emission wavelength was set by using a 450 ± 10 nm bandpass filter mounted on the fluorescence detector. The enzyme, substrate, and inhibitor concentrations were chosen so that all the reactions were under steady-state conditions. For the K_M measurements of both caspase-3 and caspase-8, the final reaction mixtures contained 10 nM enzyme. Caspase-3 inhibition experiments were performed at 10 nM enzyme and 50 μM substrate whereas caspase-8 inhibition experiments were run at 10 nM enzyme and 25 μM substrate. In a typical reaction, equal volumes (about 50 μl each) of the 2× substrate, inhibitor, and DMSO mixture and 2× enzyme in the reaction buffer were mixed rapidly on the stopped-flow apparatus. The reaction progress curve, i.e., the fluorescence emission intensity-

versus-time curve, was then monitored up to 4 min. A minimum of three curves were averaged for each substrate/inhibitor concentration, with at least six concentrations examined for each inhibitor.

2.3. Kinetic data analysis

The initial velocities (V) of the caspase-3 and caspase-8 catalyzed reactions were calculated from the slopes of the linear initial progress curves. K_M values of both enzymes toward their corresponding substrates were then determined by nonlinear least squares regression fittings of the initial velocity (V)-versus-substrate concentration ([S]) curves according to the Michaelis–Menten equation (Eq. (1)) using the program Prism (GraphPad).

$$V = \frac{V_{max}[S]}{K_M + [S]}. \quad (1)$$

Progress curves consistent with first-order inhibition kinetics (two-step irreversible inhibition mechanism; Scheme 3) were fit according to Eq. (2) by nonlinear least squares regressions to determine k_{obs} values at each inhibitor concentrations:

$$F_t = F_0 + V_0\frac{(1-e^{-k_{obs}t})}{k_{obs}}, \quad (2)$$

where F_t is the fluorescence intensity at time t, F_0 is the background fluorescence intensity, V_0 is a constant related to the steady-state rate (in fluorescence units) of the uninhibited reaction, and k_{obs} is the observed rate constant of enzyme inactivation. The inhibition or dissociation constant of the enzyme/inhibitor complex (K_I) and the first-order rate constant of inactivation at infinite inhibitor concentration (k_{inact}) values were then obtained by fitting the k_{obs}-versus-[I] curves according to Eq. (3),

$$k_{obs} = \frac{k_{inact}[I]}{[I] + K_I\left(1 + \frac{[S]}{K_M}\right)}. \quad (3)$$

Progress curves consistent with first-order, followed by a steady-state phase kinetics (slow-binding reversible inhibition mechanism; Scheme 4) were fit according to Eq. (4) by nonlinear least squares regressions to determine k_{obs} values:

$$F_t = F_0 + (V_0 - V_s)\frac{(1-e^{-k_{obs}t})}{k_{obs}} + V_s t, \quad (4)$$

where F_t, F_0, and V_0 have the same meanings as in Eq. (2) and V_s is the steady-state rate of the inhibited reactions. K_I and k_2 and k_{-2} values were then obtained by fitting the k_{obs}-versus-[I] curves according to Eq. (5),

$$k_{obs} = \frac{k_2[I]}{[I] + K_I\left(1 + \frac{[S]}{K_M}\right)} + k_{-2}. \quad (5)$$

2.4. Crystallization of caspase-3/Compound-1 complex

About 2 μl of a 100-mM DMSO stock solution of Compound-1 was added to 100 μl of caspase-3 (6.5 mg/mL in 20 mM Tris, 10 mM DTT, pH 8.0) and incubated at 4 °C for 60 minutes. The solution was centrifuged at 3000 rpm for 3 minutes before setting up sitting drops.

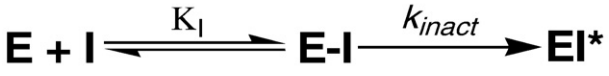

Scheme 3. A two-step irreversible inhibition mechanism.

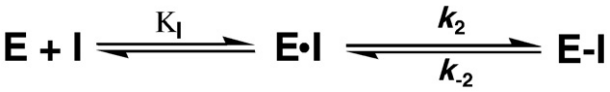

Scheme 4. A two-step slow binding reversible inhibition mechanism.

Crystals of caspase-3 in the presence of Compound-1 were grown by vapor diffusion at 4 °C from 5-μl drops containing equal volumes of 16% ethanol, 0.1 M Tris buffer at pH 7.8 and the protein complex solution.

2.5. Crystallization of caspase-8/inhibitor complexes

About 2.0 μl of 100-mM stocks of MMX inhibitors (Compound-4 or Compound-9) dissolved in DMSO were added to 100-μl aliquots of 8.4 mg/ml caspase-8 (0.30 mM) in 20 mM Tris, 100 mM DTT, pH 8.0. The protein/inhibitor solutions were incubated at 4 °C for 60 minutes. The solutions were then centrifuged at 3000 rpm for 3 minutes before setting up the sitting drops. Drops of 2.5 μl were mixed with an equal volume of reservoir solution [1.0–1.1 M citrate, 0.1 M HEPES (or PIPES), pH 6.5] and incubated at 4 °C. The average size of the crystals was 0.2 × 0.2 × 0.3 mm.

2.6. Crystallographic data collection and refinement

The caspase-3 crystals were flash frozen directly in liquid nitrogen. The caspase-8 crystals were slowly introduced to cryoprotectant before freezing (final solution: 1.0 M citrate, 50 mM HEPES (or PIPES), pH 6.5, and 25 mM DTT). The data sets were collected at the Advanced Photon Source (APS; Argonne National Laboratory, Argonne, IL) IMCA-CAT beamlines and scaled with the *HKL2000* software package [52]. The data collection and refinement statistics are given in Table 2. The structures of the complexes were solved by molecular replacement using the program AMoRe in the CCP4 program suite [53,54]. The caspase-3 complexes were solved with a search model based on the published caspase-3 (1CP3 in the Brookhaven Data Bank) structure [32]. Some of the caspase-8 complexes were solved with a search model based on the caspase-8/Ac-IETD-H structure [38]. Refinements were carried out by alternating rounds of refinement using SHELXTL97 [55], CNX, 2002 (Accelrys, San Diego, CA) or REFMAC [53,56], with manual rebuilding using CHAIN, LORE, or COOT [57–59]. Parameter files generated using the software package Afitt (Openeye Scientific Software, Santa Fe, NM) were manually edited prior to use. All structures were checked for integrity using PROCHECK [60].

3. Results

3.1. Steady-state kinetic parameters (K_M)

Steady-state kinetic analyses of caspase-3- and caspase-8-catalyzed reactions in the absence of inhibitors were first carried out to determine K_M values for both enzymes toward their respective substrates. Under the experimental conditions, both enzymes followed Michaelis–Menten kinetics (data not shown). K_M values of 33.7 ± 3.9 μM and 4.52 ± 0.47 μM were obtained for the caspase-3 and caspase-8 reactions, respectively.

3.2. Stopped-flow kinetics of caspase inhibition by Z-VAD-fmk

Caspase-3-catalyzed Ac-DEVD-AMC hydrolysis reactions were measured in the presence of 0, 1, 2, 5, 10, 20, 40, 80, 150, and 300 μM Z-VAD-fmk (Fig. 1) and a series of progress curves (fluorescence intensity vs. time) were obtained (Fig. 2A). It was noted that the progress curve at 0 μM Z-VAD-fmk was slightly curved. Simulation of caspase-3 reaction progress using the determined kinetic parameters

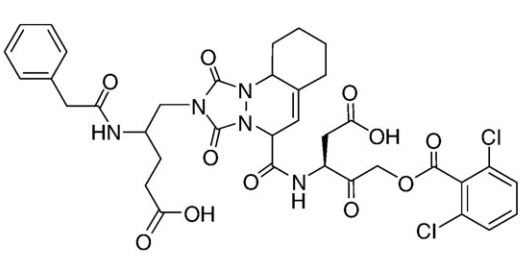

Compound 1

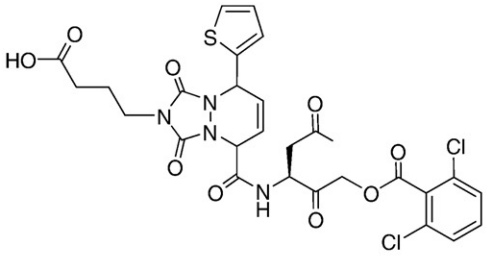

Compound 2

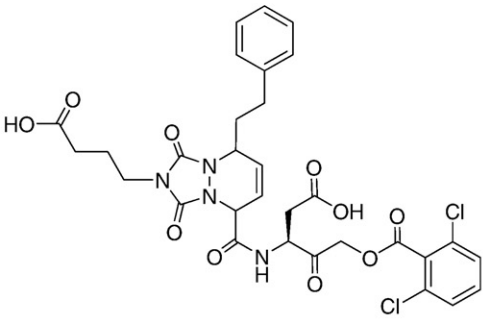

Compound 3

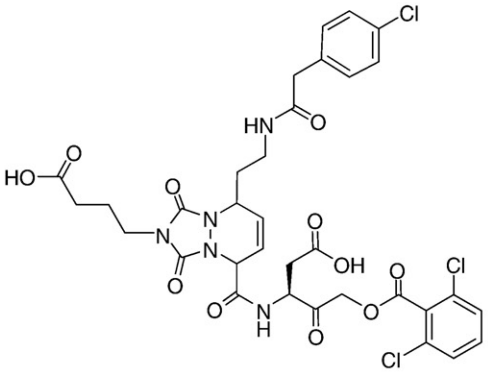

Compound 4

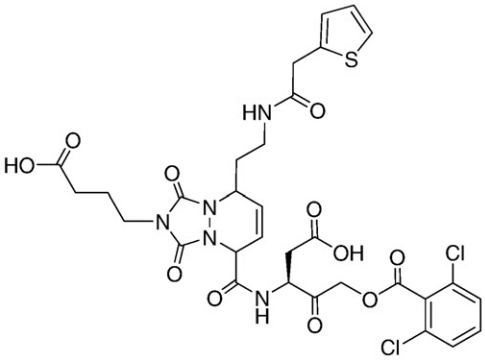

Compound 5

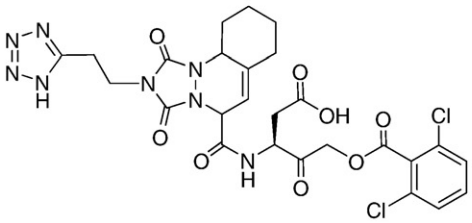

Compound 6

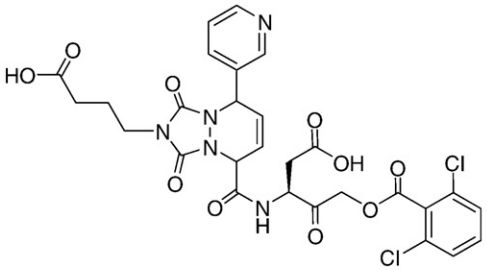

Compound 7

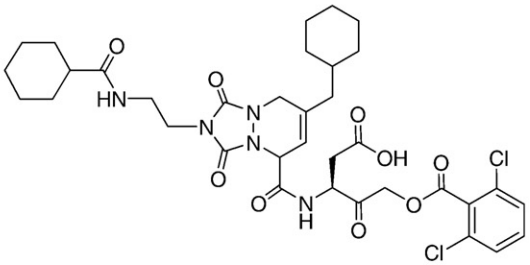

Compound 8

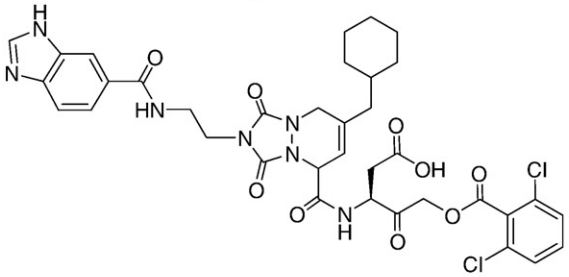

Compound 9

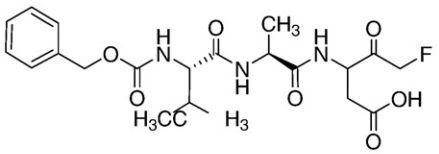

Z-VAD-fmk

Fig. 1. Chemical structures of selected peptidomimetic caspase inhibitors.

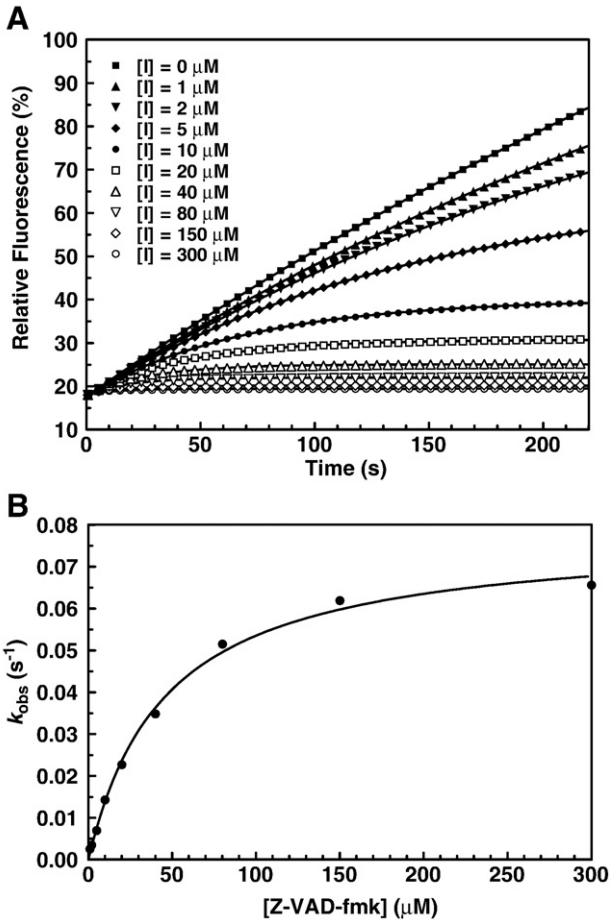

Fig. 2. Caspase-3 inhibition by Z-VAD-fmk. A. Progress curves of Ac-DEVD-AMC hydrolysis catalyzed by caspase-3 in the presence of various concentrations of Z-VAD-fmk as indicated. The data were obtained under the conditions described in the Materials and methods section (50 μM substrate and 10 nM enzyme) and analyzed according to Eq. (2). B. Values of k_{obs} obtained from panel A plotted versus Z-VAD-fmk concentrations. The plot was fit according to Eq. (3) to generate K_I and k_{inact} values.

with Program DYNAFIT [61] ruled out measurable substrate depletion during the 240-second data acquisition period, suggesting that caspase-3 undergoes autoinactivation at a low concentration. The progress curves at different Z-VAD-fmk concentrations appeared to be first order, consistent with an irreversible inhibition mechanism (Scheme 3). Eq. (2) was successfully fit to these curves by nonlinear least squares regression (Fig. 2A), and k_{obs} values at different inhibitor concentrations were obtained (Fig. 2B). The k_{obs}-versus-inhibitor curve approaches saturation at high inhibitor concentrations. This allows the K_I and k_{inact} values of caspase-3 inhibition by Z-VAD-fmk to be determined unambiguously by fitting the data according to Eq. (3) (Fig. 2B). The K_I and k_{inact} of the inhibition of caspase-3 by Z-VAD-fmk are 18.4 ± 1.4 μM and 0.078 ± 0.002 s^{-1}, respectively (Table 1).

Inhibition studies of caspase-8 by Z-VAD-fmk were also carried out and the progress curves obtained at different inhibitor concentrations are shown in Fig. 3A. The linear progress curve at 0 μM inhibitor demonstrated that caspase-8 is stable at low concentration. Similar to the caspase-3 study, the progress curves in the presence of Z-VAD-fmk are first order. However, much less inhibitor was required to inhibit caspase-8 to the same extent as caspase-3. This suggests that Z-VAD-fmk is a more potent inhibitor for caspase-8. Fitting Eq. (2) to the progress curves (Fig. 3A), a k_{obs}-versus-inhibition concentration curve was obtained (Fig. 3B). This curve shows saturable behavior at high Z-VAD-fmk concentrations and K_I of 0.45 ± 0.05 μM and k_{inact} of 0.23 ± 0.01 s^{-1} were determined by fitting the data according to Eq. (3) (Fig. 3B).

3.3. Caspase inhibition by the MMX irreversible inhibitors

The chemical structures of selected irreversible inhibitors and their inhibition kinetic parameters against caspase-3 and caspase-8 are summarized in Fig. 1 and Table 1, respectively. When the caspase-3-catalyzed Ac-DEVD-AMC hydrolysis reactions were measured in the presence of 0, 0.2, 0.5, 1, 2, 5, 10, and 20 μM Compound-6, progress curves similar to those in the presence of Z-VAD-fmk were obtained (Fig. 4A). The first-order progress curves fit Eq. (2) well (Fig. 4A), and k_{obs} values at different Compound-6 concentrations were obtained (Fig. 4B). K_I of 13.4 ± 3.7 μM and k_{inact} of 0.094 ± 0.018 s^{-1} were calculated by fitting the k_{obs}-versus-Compound-6 concentration curve according to Eq. (3) (Fig. 4B).

Similar experiments were carried out on caspase-8 inhibition by Compound-6, and the progress curves at different Compound-6 concentrations are shown in Fig. 5A. The linear progress curve at 0 μM Compound-6 concentration again confirms the stability of caspase-8 at low concentration. However, none of the progress curves obtained in the presence of the inhibitor is first-order. They all exhibit an initial "burst" phase followed by a steady-state increase of the signal. This behavior is consistent with a slow-binding reversible inhibition model (Scheme 4). In fact, all the progress curves can be fit nicely according to Eq. (4) (Fig. 5A) to generate an array of k_{obs} values (Fig. 5B). The k_{obs}-versus-Compound-6 concentration curve exhibited saturation behavior at high inhibitor concentrations and K_I, k_2, and k_{-2} values were determined unambiguously using Eq. (5) (Fig. 5B). The kinetic parameters of caspase-8 inhibition by Compound-6 are as follows: $K_I = 9.27 \pm 1.03$ μM, $k_2 = 0.18 \pm 0.01$ s^{-1}, and $k_{-2} = 0.043 \pm 0.007$ s^{-1}.

Inhibition of caspases-3 and -8 by more than three dozen other irreversible MMX inhibitors was also examined using the stopped-flow technique. It was found that all the compounds behave like Compound-6, i.e., they act like two-step irreversible inhibitors for caspase-3 and slow-binding reversible inhibitors for caspase-8.

3.4. Caspase/inhibitor co-crystal structures

We have determined the structures of three caspase bound peptidomimetic inhibitors. Compound-1 bound to caspase-3 crystallized in space group $P2_12_12$ and yielded data to a resolution of 2.0 Å. Compound-4 and Compound-9 bound to caspase-8 crystallized in a trigonal crystal form ($P3_121$) previously reported by Watt et al. [38] and yielded data sets to 1.8 Å resolution. The structures have been refined to crystallographic R values of 17.0% to 18.6% (R_{free} 21.0–22.6%). Compound structures are illustrated in Fig. 6 with R1, R2, and R3 representing substitution groups at the 1, 4, and 5 positions, respectively. Summaries of the diffraction data and crystallographic refinement statistics are presented in Table 2.

These structures agree well with previously determined caspase-3 and caspase-8 structures. Calculated over all pairs of C_α atoms in the structures, the RMSD between the caspase-3 structure described here and that of an Ac-DVAD caspase-3 complex [32] is 0.3 Å. The similarly calculated RMSDs between the Compound-4 and Ac-IETD [38], or Compound-9 and Ac-IETD bound caspase-8 structures are 0.3 and 0.2 Å, respectively. The inhibitors described here thus do not induce global, novel protein conformational changes.

The interpretation of the electron density maps and analysis of bound ligand geometry was aided by the high resolution of the data (Fig. 7 and Table 2). Given the long timescale of crystallographic experiments, it is unsurprising that the reactions proceeded through to the irreversible loss of the dichlorobenzoate moiety. There is thus no evidence of the 2,5-dichlorobenzoate leaving group in any of the electron density maps. For the caspase-3 complex structure, and the structure of Compound-9 bound to caspase-8, all other inhibitor atoms are visible in the electron density. In the Compound-4/caspase-8 structure, although the urazolopyridazine core is well ordered, the R3 group (a 4-chlorophenyl acetic acid amide methylene moiety) is

Table 1
Inhibition constants for caspases-3 and -8 by selected inhibitors.

Caspase-3					
Inhibitors	K_I (μM)	k_2 (s^{-1})	k_{-2} (s^{-1})	k_{inact} (s^{-1})	k_{inact}/K_I (M^{-1} s^{-1})
Z-VAD-fmk	18.4 ± 1.4	N/A[a]	N/A	0.078 ± 0.002	4,200
Compound-1	13.4 ± 3.7	N/A	N/A	0.094 ± 0.018	7,000
Compound-2	9.13 ± 1.01	N/A	N/A	0.082 ± 0.004	9,000
Compound-3	0.66 ± 0.02	N/A	N/A	0.058 ± 0.001	88,000
Compound-4	5.05 ± 0.32	N/A	N/A	0.082 ± 0.002	16,000
Compound-5	5.24 ± 0.39	N/A	N/A	0.074 ± 0.002	14,000
Compound-6	2.03 ± 0.25	N/A	N/A	0.067 ± 0.003	33,000
Compound-7	6.81 ± 1.20	N/A	N/A	0.086 ± 0.007	13,000
Compound-8	7.54 ± 0.68	N/A	N/A	0.026 ± 0.001	3,400
Compound-9	17.2 ± 1.6	N/A	N/A	0.023 ± 0.001	1,300
Caspase-8					
Inhibitors	K_I (μM)	k_2 (s^{-1})	k_{-2} (s^{-1})	k_{inact} (s^{-1})	$K_I[k_{-2}/(k_{-2}+k_2)]$ (μM)
Z-VAD-fmk	0.45 ± 0.03	N/A	N/A	0.23 ± 0.01	N/A[b]
Compound-1	9.27 ± 1.03	0.18 ± 0.01	0.004 ± 0.001	E/S[c]	0.202
Compound-2	0.33 ± 0.13	0.16 ± 0.01	<0.009	E/S	<0.018
Compound-3	3.54 ± 0.88	0.45 ± 0.08	0.011 ± 0.002	E/S	0.084
Compound-4	1.32 ± 0.12	0.18 ± 0.01	0.007 ± 0.002	E/S	<0.049
Compound-5	1.52 ± 0.54	0.19 ± 0.02	<0.009	E/S	0.069
Compound-6	3.63 ± 0.15	0.14 ± 0.01	0.008 ± 0.001	E/S	0.196
Compound-7	3.10 ± 0.22	0.56 ± 0.02	0.012 ± 0.002	E/S	0.065
Compound-8	3.57 ± 0.33	0.21 ± 0.01	<0.003	E/S	<0.050
Compound-9	6.44 ± 0.29	0.54 ± 0.02	0.004 ± 0.001	E/S	0.047

[a] Not available.
[b] $k_{inact}/K_I = 510{,}000$ M^{-1} s^{-1}.
[c] Extremely slow (<0.005 s^{-1}).

not visible and presumably disordered. In all three structures, the electron density is very clear for the catalytic cysteine sulfur atom and for the proximal ketone moiety. There is continuous electron density connecting the ketone with the sulfur atom, confirming the existence of a covalent bond. We have placed the methylene carbon atom linking the ketone to the sulfur in a position consistent with geometric constraints, although the electron density is perhaps somewhat weaker than might be expected. It is unlikely that the methylene group would be more mobile than its neighboring atoms, and so the weaker electron density is most parsimoniously explained by a limited degree of chemical heterogeneity in this region of the structure. Radiation decay due to X-ray exposure during data collection has previously been shown to be responsible for the modification of a thiomethylketone in the active site of a caspase-3 structure determined at 1.06 Å resolution [62]. A similar phenomenon may be occurring in the structures described here. The identities of the alternate species could not be unambiguously determined either in the atomic resolution structure of capsase-3 or in those described here.

3.5. Caspase/inhibitor interactions

The inhibitors share a number of common interactions with caspase-3 and -8 in addition to their covalent linkage to the catalytic cysteine. In all three adducts the "warhead" ketone oxygen hydrogen bonds with the backbone amide NH of both the catalytic cysteine and conserved glycine (caspase-3 Gly^{122}, caspase-8 Gly^{318}). Similarly, the P_1 carboxylate moiety forms hydrogen bonds with the side chains of three conserved residues (caspase-3 Arg^{64}, caspase-8 Arg^{260}; caspase-3 Arg^{207}, caspase-8 Arg^{413}; caspase-3 Gln^{161}, caspase-8 Gln^{358}). The adjacent amide nitrogen hydrogen bonds with a main chain carbonyl (caspase-3 Ser^{205}, caspase-8 Ser^{411}) as well as forming a close contact with the catalytic cysteine sulfur atom (3.0 Å). One of the carbonyls of the urazolopyridazine forms a hydrogen bond with a backbone main chain amide (caspase-3 Arg^{207}, caspase-8 Arg^{413}). As can be surmised from this enumeration of interactions, the structures show that the core elements of the inhibitors bind to caspase-3 and caspase-8 in similar ways. These interactions closely mimic those of caspases with peptidic substrates (Fig. 8).

Beyond these core regions, the different MMX inhibitors mimic different elements of caspase peptide substrates. For example, the butyrate moiety in Compound-4 superimposes well on the P_3 glutamic acid of the Ac-IETD caspase-8 structure (Fig. 8). Indeed, both of these moieties hydrogen bond with their neighboring waters in an identical fashion. In contrast, Compound-9 lacks a glutamic acid mimic, but has an amide nitrogen in the R1 position where it forms a hydrogen bond with Arg^{413}. Compound-9 also forms a hydrogen bond between an oxygen atom from the urazolopyridazine moiety and the amide nitrogen of Arg^{413}. It thus matches the antiparallel backbone hydrogen bonding interactions observed between the P_3 glutamic acid and Arg^{413} in the Ac-IETD caspase-8 structure. A similar pattern of interactions is apparent when the structures of Compound-1 and Ac-DVAD in caspase-3 are compared. Of course, in addition to mimicking peptide substrates, the MMX inhibitors also form novel interactions with the caspases, such as those of the benzimidazole moiety of Compound-9 with caspase-8.

3.6. Compound-4 also binding to caspase-8 in a pocket far from the active site

In addition to covalent binding at the active site, Compound-4 also binds noncovalently close to the interface between two p18–p11 heterodimers (Fig. 9). One ring of the urazolopyridazine and the R3 group that emerges from this ring (a 4-chlorophenyl acetic acid amide ethylene moiety) are clearly visible in the electron density. The urazolopyridazine binds to a relatively flat and featureless surface of the protein. The oxygen of the amide forms a hydrogen bond with the side chain of Glu^{396} while the nitrogen forms a hydrogen bond with the side chain of Thr^{337}. The chlorophenyl moiety occupies a well-defined, hydrophobic pocket, stacking on Phe^{399} and forming an edge to face interaction with Tyr^{334}.

When compared with other caspase-8 structures, it is apparent that the presence of Compound-4 appears to induce a conformational

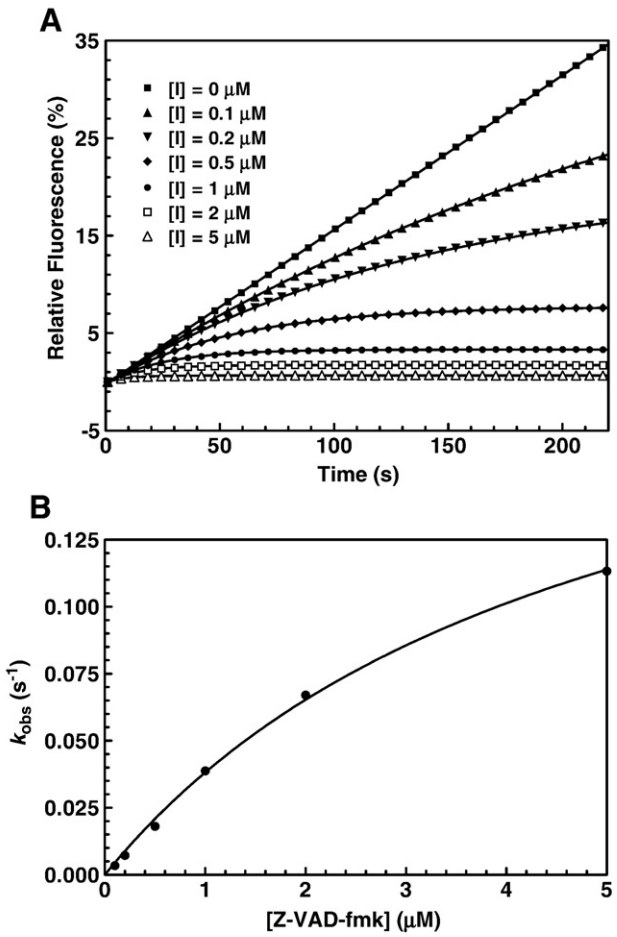

Fig. 3. Caspase-8 inhibition by Z-VAD-fmk. A. Progress curves of Ac-IETD-AMC hydrolysis catalyzed by caspase-8 in the presence of various concentrations of Z-VAD-fmk as indicated. The data were obtained under the conditions described in the Materials and methods section (25 μM substrate and 10 nM enzyme) and analyzed according to Eq. (2). B. Values of k_{obs} obtained from panel A plotted versus Z-VAD-fmk concentrations. The plot was fit according to Eq. (3) to generate K_I and k_{inact} values.

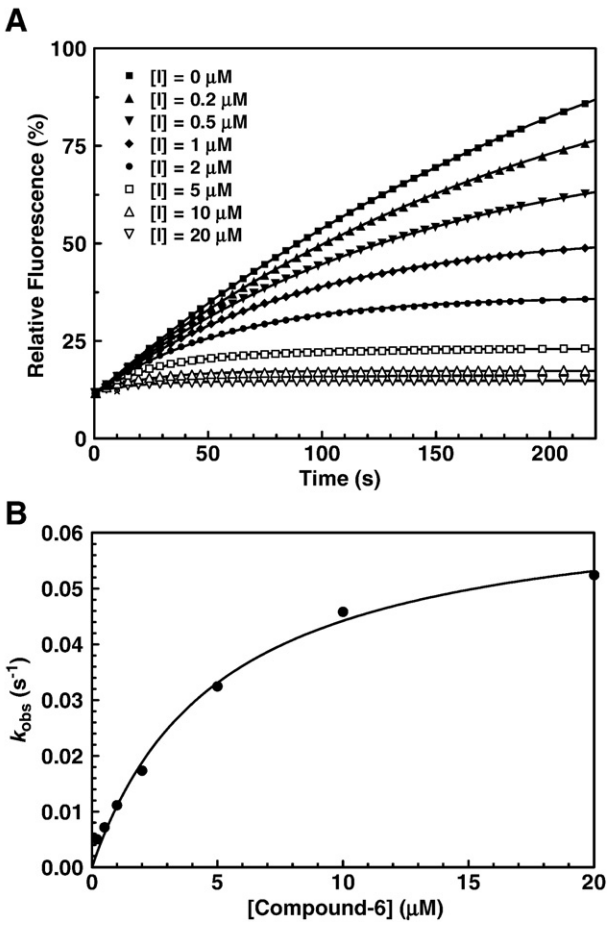

Fig. 4. Caspase-3 inhibition by Compound-6. A. Progress curves of Ac-DEVD-AMC hydrolysis catalyzed by caspase-3 in the presence of various concentrations of Compound-6 as indicated. The data were obtained under the conditions described in the Materials and methods section (50 μM substrate and 10 nM enzyme) and analyzed according to Eq. (2). B. Values of k_{obs} obtained from panel A plotted versus Compound-6 concentrations. The plot was fit according to Eq. (3) to generate K_I and k_{inact} values.

change in this pocket. In the structure of caspase-8 bound to Ac-IETD-aldehyde [38], the pocket is occupied by an oxidized molecule of DTT, and Tyr^{334} is in an alternate rotomeric state. This tyrosine is also in this alternate rotomeric state in the structure of caspase-8 bound to Compound-9, where the pocket is occupied by a reduced DTT molecule. This alternate tyrosine rotomer is incompatible with the binding of Compound-4 as the tyrosine would clash with the urazolopyridazine moiety.

4. Discussion

This study presents a detailed kinetic analysis of the inhibition of caspase-3 and caspase-8 by a series of irreversible inhibitors that form thioether bonds with the active site thiol. Moreover, the structures of three of the resulting covalently modified caspase derivatives have been solved by X-ray crystallography, providing a glimpse into the catalytic sites of these important enzymes.

4.1. Stopped-flow kinetic studies of caspase inhibition by irreversible inhibitors

To achieve potent inhibition of cysteinyl proteases, it has been necessary to make inhibitors containing an electrophilic group to enable the formation of a covalent bond with the active site thiol. Here, this principle has been successfully applied to the development of potent irreversible peptidomimetic inhibitors of caspase-3 and caspase-8. Kinetic analysis of irreversible enzyme inhibition is complicated by the fact that it is usually a multi-step process; kinetic parameters of each step are required to describe the inhibition kinetic mechanism. Previous kinetic studies of irreversible caspase-3 and caspase-8 inhibitors failed to determine the individual kinetic parameters; only k_{inact}/K_I values were obtained. As we observed from this work, the inhibition processes of caspase-3 and caspase-8 by irreversible inhibitors were usually fast at high inhibitor concentrations so that after a very short time, virtually no substrate was turning over. The consequence is that the product release progress curve exhibited an extremely short first-order portion before becoming saturated (irreversible) or entering the linear steady-state stage (reversible). This makes the determination of the k_{obs} values at high inhibitor concentrations extremely difficult. Without k_{obs} values at high inhibitor concentrations, it is impossible to determine each individual inhibition kinetic parameter (K_I and k_{inact} in the two-step irreversible and K_I, k_2, and k_{-2} in the slow-binding reversible mechanism described in Schemes 3 and 4, respectively) by nonlinear least squares regression fittings using Eq. (3) or (5). In this work, we employed a stopped-flow apparatus to acquire the progress curves so that the k_{obs} values at high inhibitor concentrations were determined accurately. Our stopped-flow system generated reliable data for AMC release from both the caspase-3- and caspase-8-catalyzed reactions in the presence of Z-VAD-fmk and the irreversible MMX inhibitors. The mathematical models fit the corresponding progress curves well and a

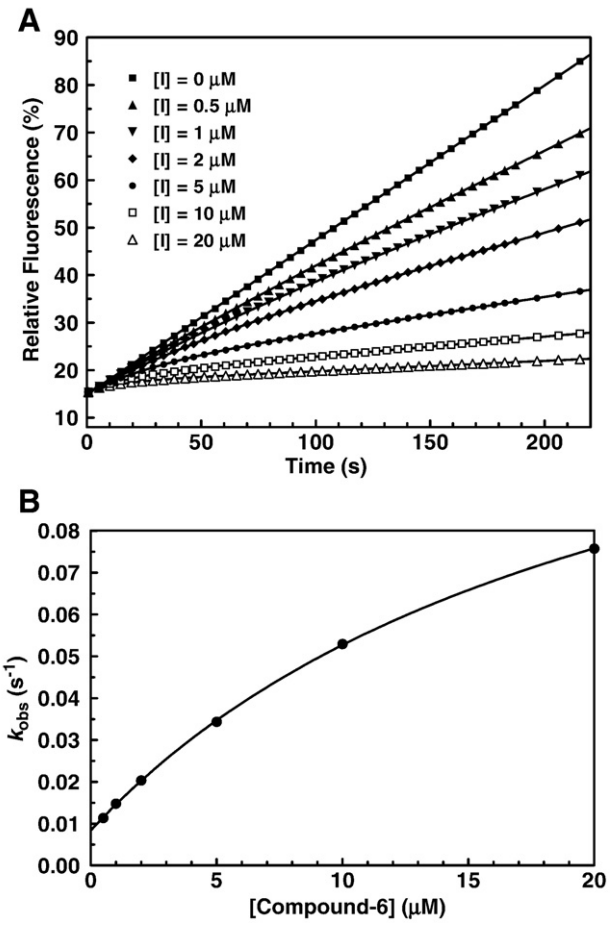

Fig. 5. Caspase-8 inhibition by Compound-6. A. Progress curves of Ac-IETD-AMC hydrolysis catalyzed by caspase-8 in the presence of various concentrations of Compound-6 as indicated. The data were obtained under the conditions described in the Materials and methods section (25 μM substrate and 10 nM enzyme) and analyzed according to Eq. (4). B. Values of k_{obs} obtained from panel A plotted versus Compound-6 concentrations. The plot was fit according to Eq. (5) to generate K_I, k_2, and k_{-2} values.

saturable k_{obs}-versus-inhibition concentration ([*I*]) curve was obtained for each enzyme-inhibitor pair. Fitting k_{obs}- versus-[I] curves according to the relevant equations, we were able to obtain all the individual kinetic parameters involved in two-step irreversible inhibition (caspase-3 and -8 inhibition by Z-VAD-fmk and caspase-3 inhibition by Compound-6 and other irreversible peptidomimetic inhibitors) and slow-binding reversible inhibition (caspase-8 inhibition by Compound-6 and other irreversible peptidomimetic inhibitors; Table 1).

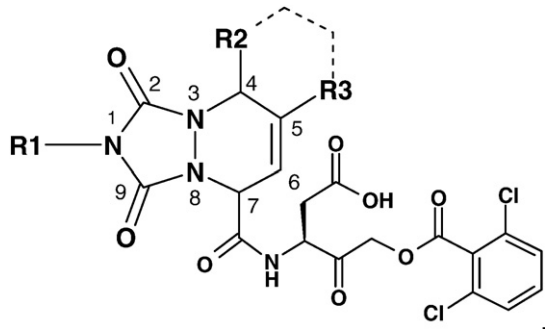

Fig. 6. Representation of the substitution groups, R1, R2, and R3, in MMX compounds, especially the carbocyclic fusion of R2 and R2 utilized in inhibitors such as Compound-1 and Compound-6.

Table 2
Summary of crystallographic statistics.

Protein	Caspase-8	Caspase-8	Caspase-3
Compound	Compound-9	Compound-4	Compound-1
Space group	$P3_121$	$P3_121$	$P2_12_12$
Unit cell dimensions	62.6, 62.6, 129.39, 90.0, 90.0, 120.0	64.0, 64.0, 130.9, 90.0, 90.0, 120.0	96.69, 68.2, 44.8, 90.0, 90.0, 90.0
No. of molecules in A.S.	1	1	1
Resolution	20.0–1.8 (1.85–1.80)	20.0–1.8 (1.85–1.80)	20–2.0 (2.05–2.0)
I/sigma	13.8 (2.9)	13.8 (2.9)	19.7 (4.3)
Completeness	95.7 (81.7)	99.6 (96.9)	89.2 (60.2)
rmsd bond length,	0.007	0.009	0.009
Rmsd angles	1.20	1.24	1.35
R_{cryst}	17.0 (21.0)	18.5 (24.1)	18.3 (23.8)
R_{free}	20.2 (21.8)	20.8 (29.3)	20.6 (23.7)
PDB ID code	3KJN	3KJQ	3KJF
Ramachandran			
Core	89.5	89.5	91.7
Allowed	10.5	10.5	8.3
Generous	0	0	0
Disallowed	0	0	0

The values in parentheses are for the high-resolution shell.

The unambiguous determination of these parameters makes it possible for us to compare the potencies of irreversible caspase inhibitors in ways that have not previously been possible. For example, Table 1 includes the calculation of k_{inact}/K_I for caspase-3 inhibitors and $K_I[k_{-2}/(k_{-2}+k_2)]$ for caspase-8 inhibition. These values can be viewed as the overall second-order rate constant for the irreversible inhibition of caspase-3 and the overall K_i for the reversible phase of caspase-8 inhibition, respectively. It is of interest that for Compounds 1–9 k_{inact}/K_I for caspase-3 inhibition correlates very well with $1/K_I$ ($R^2 = 0.9865$). There is no correlation between k_{inact}/K_I and k_{inact} ($R^2 = 0.0007$). This suggests that the overall potency of these compounds for caspase-3 is driven primarily by the rapidly reversible affinity component, K_I, instead of by differences in k_{inact}. Examination of Table 1 confirms that while k_{inact}/K_I varies 66-fold for these compounds, k_{inact} varies only 4-fold, but K_I varies 23-fold. A similar analysis of caspase-8 inhibition by these compounds is not possible,

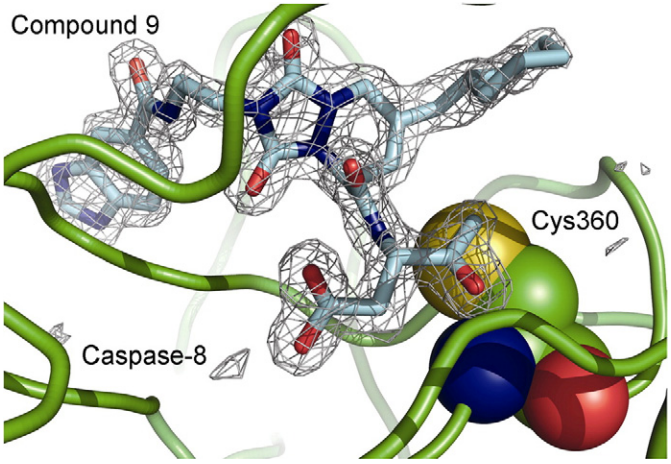

Fig. 7. Electron density map for Compound-9 bound to caspase-8. The gray mesh is 3 standard deviations above the mean contour in a weighted Fo–Fc electron map phased using a model with inhibitor omitted and calculated from 20.0 to 1.8 Å resolution. The catalytic cysteine is shown using spheres. Protein main chain is indicated using a green ribbon trace. Figs. 6–8 were made using PyMol Molecular Graphics System (DeLano Scientific, San Carlos, CA).

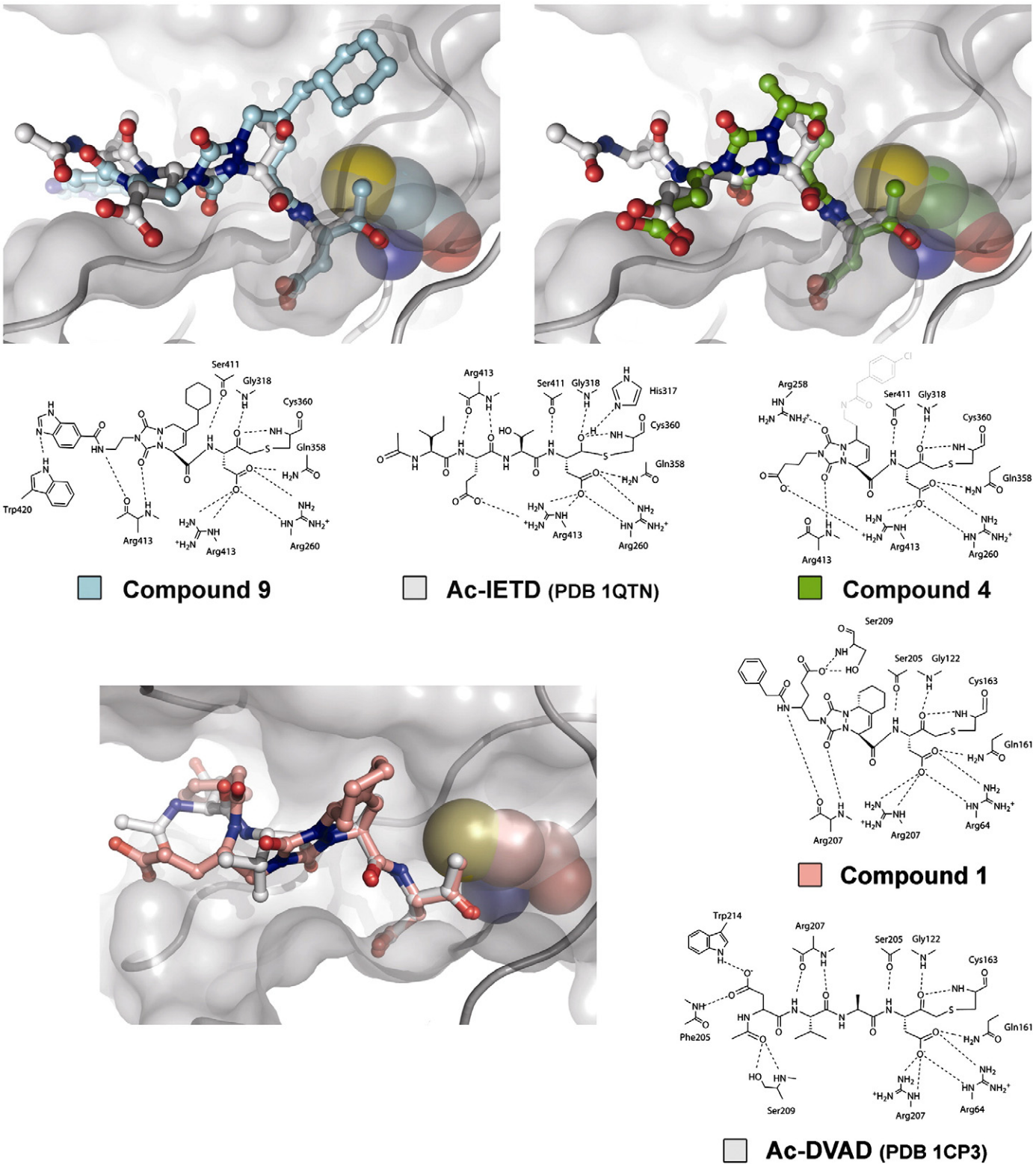

Fig. 8. Comparison of MMX and peptidic inhibitors. The peptide mimicry of the MMX inhibitors is illustrated by superposing the caspase C_α atoms in peptidic inhibitor- and MMX-containing structures. The ribbon trace and protein surface of the peptidic inhibitor complexes are shown in gray, and the inhibitors themselves are shown in white and colored ball-and-stick representation. The catalytic cysteines are shown as spheres, and the MMX inhibitors are shown in colored ball-and-stick representation. The chemical diagrams indicate hydrogen bonding interactions (dashed lines). A disordered 4-chlorophenyl acetic acid amide methylene moiety in Compound-4 is shown in the diagram in gray. Hydrogen bonds with water have been omitted for clarity. The P_3 carboxylate of Ac-IETD forms two water interactions with Asn^{261} and Asp^{259} in caspase-8; the identical interactions are formed by the butyrate moiety of Compound-4.

since k_{inact}/K_I is not known. However, if the structure–activity relationships for caspase-3 and caspase-8 inhibition were similar, one might expect either $1/K_I$ or $1/K_i([k_{-2}/(k_{-2}+k_2)]$ for caspase-8 inhibition to correlate with k_{inact}/K_I for caspase-3. These correlations are very poor, however ($R^2 = 0.0259$ and 0.0600, respectively), suggesting that Compounds 1–9 may have different structure–activity

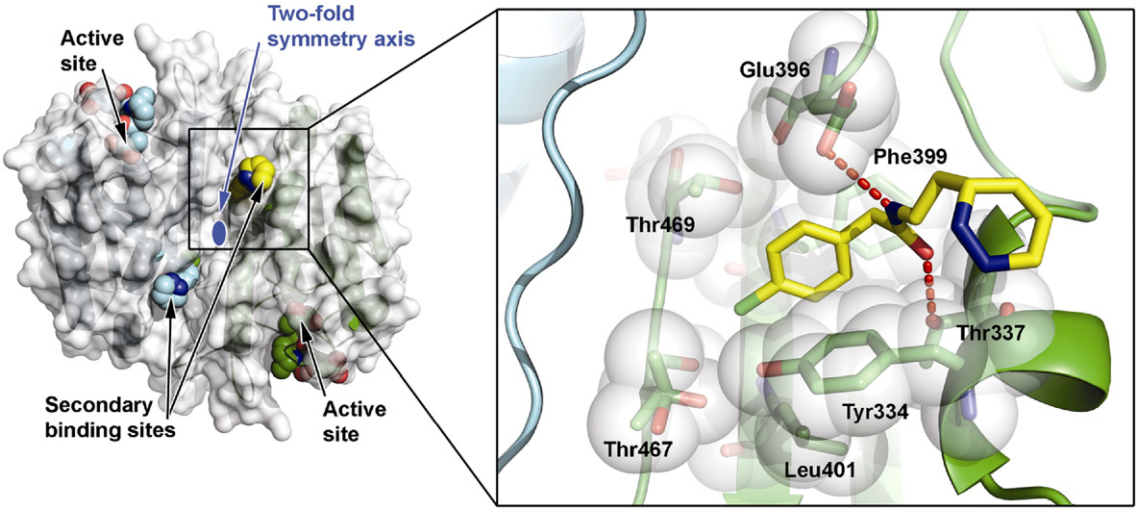

Fig. 9. Inhibitor binding at a secondary pocket in caspase-8. An overall view of the biological dimer of heterodimers of caspase-8 with Compound-4 is shown on the left. A two-fold symmetry axis projecting out of the plane of the page is indicated by a blue oval. Beneath the surface, one heterodimer is shown with a cyan cartoon, and the other with a green cartoon. Ligands bound at the active site and secondary binding sites are shown in sphere representation. A zoomed-in view of one of the secondary binding sites is shown on the right. The ligand is shown in stick representation, with carbon atoms colored yellow. Residues that form the binding pocket are shown as sticks and transparent spheres with carbon atoms colored green. The heterodimer subunits are colored in the same way as in the overall view on the left. Hydrogen bonds are indicated by dashed red lines.

relationships for caspase-3 and 8 inhibition and that selective inhibition of these enzymes by this class of inhibitors may be possible. Indeed, Table 1 suggests that Compound-3 is the most potent inhibitor of caspase-3, but one of the three weakest inhibitors of caspase-8, while the most potent inhibitor of caspase-8 (Compound-2) is among the four weakest inhibitors of caspase-3.

4.2. Kinetic mechanism of caspase inhibition by irreversible inhibitors

Z-VAD-fmk is a widely used irreversible caspase inhibitor. Like Compound-6 and the other irreversible peptidomimetic inhibitors, the irreversible modification could take place via one of the two pathways shown in Scheme 5. Both mechanisms consist of the rapid formation of a noncovalent enzyme-inhibitor (Michaelis) complex ($E \cdot I$) and the possibility of the formation of a thiohemiketal intermediate (E-I). They differ in the route by which the cysteine residue of the enzyme active site reacts to form a thioether product (EI^*) with the concomitant release of the leaving group (fluoride from Z-VAD-fmk and dichlorobenzoate from the peptidomimetic inhibitors). In one case (path B in Scheme 5), the Michaelis complex leads to direct attack of the methylene carbon by the active site cysteine residue to form the thioether product (EI^*). In the other case (path A in Scheme 5), the thiohemiketal is the immediate precursor to this final product, either directly as shown or via a thiiranium ion

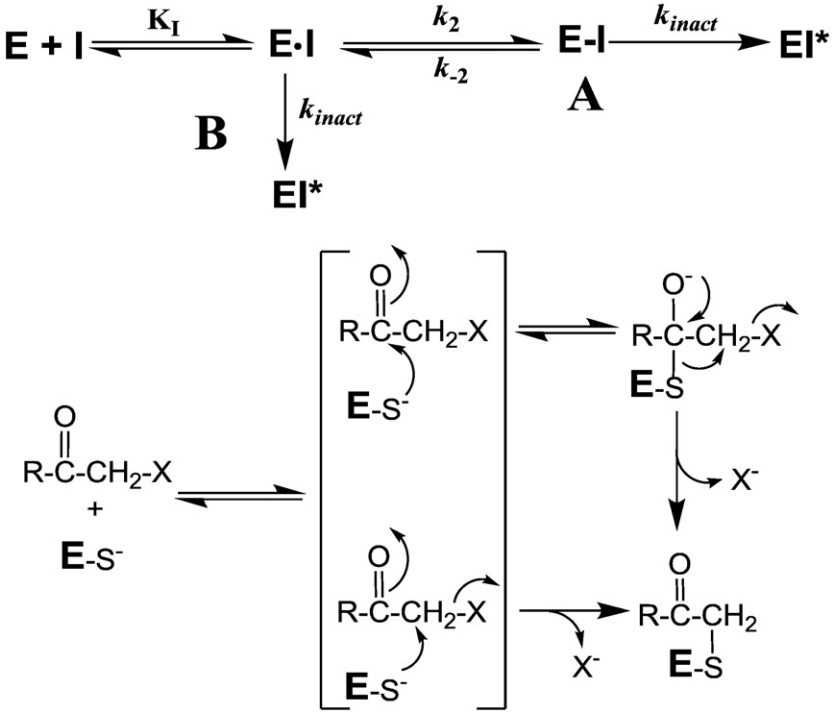

Scheme 5. A three-step irreversible inhibition mechanism.

intermediate. We cannot rule out either mechanism with just the kinetic data, and to our knowledge, there is no literature precedent to favor one over the other. Given that either of these pathways may be possible, the question arises: why do we observe only two-step inhibitory kinetic mechanisms? More specifically, why does Z-VAD-fmk inhibition of both caspases follow the two-step irreversible kinetic mechanism described by Scheme 3, while the MMX compounds follow the same kinetics in caspase-3 inhibition, but fit a two-step slow-binding reversible mechanism in caspase-8 inhibition (Scheme 4)? The answer may be found, in part, by comparing the kinetic schemes. Schemes 3 and 4 are actually subsets of the more general mechanism in Scheme 5. For example, if the rate constants k_2 and k_{-2} of Scheme 5 are large enough, as we believe is the case with Z-VAD-fmk inhibition and inhibition of caspase-3 by the peptidomimetic compounds, then the formation of the thiohemiketal becomes very fast and its formation and that of the Michaelis complex approximate a single rapid equilibrium step. In this case, Scheme 5 would be indistinguishable from Scheme 3, no matter how the final thioether is formed. On the other hand, if the rate constants k_2 and k_{-2} are small and k_{inact} is extremely small in Scheme 5, as we believe is the case with MMX compound inhibition of caspase-8, then thiohemiketal formation could not be combined in one rapid equilibrium step and the final thioether formation would not be observable under our experimental conditions. Scheme 5 would simplify to Scheme 4. The crystallographic results, which show the absence of the leaving group, demonstrate that in this latter case, the unobserved rate constant, k_{inact}, must nonetheless be present. Thus, the data are all consistent with Scheme 5, the apparent differences being due solely to the magnitudes of the individual rate constants.

4.3. Enzyme active site–inhibitor interactions

As detailed in the Results section, the urazolopyridazine inhibitors described here mimic the peptide substrates of caspases. For some of the moieties in the inhibitors, the nature of this mimicry is apparent from inspection of their chemical structures. Thus the conserved ketone warhead, P_1 aspartic acid, and amide moiety emerging from the C7 ring atom of the inhibitors has an identical counterpart in peptidic caspase substrates. Fig. 8 shows that the corresponding atoms are superimposable. Perhaps more subtly, the correspondence between inhibitors and peptidic substrates also extends to the bicyclic cores. For example, as designed, the interaction of C9 carbonyl oxygen with a conserved arginine parallels a peptidic P_3 backbone-carbonyl interaction (Fig. 8). Substitutions off the N1 position of the urazole ring allow the inhibitors to access the S_3, S_4, and S_5 pockets, and afford opportunities both to mimic peptide substrates and design novel interactions. On the basis of positional scanning using a combinatorial substrate library, Thornberry et al. [63] identified a glutamic acid as the optimal group for the P_3 position of caspase inhibitors. This preference can be explained structurally by pointing to the hydrogen bond that exists between the P_3 carboxylate in the Ac–IETD peptide complex with caspase-8 [38], and the exposed face of the conserved guanidinium of Arg^{413} (Fig. 8). The butyrate side chains that emerge from the N1 position of the urazole ring in Compounds-4 and -9 are nearly ideal mimics of this glutamic acid. In contrast, although the branched valerate of Compound-1 was designed to afford a similar interaction, the carboxylic moiety instead binds to Ser^{209} of caspase-3. Superposition of the two inhibitors suggests that replacing the valerate with a butyrate moiety may restore S_3 pocket binding. However, there appears to be little correlation in potency accompanying the presence or absence of this particular S_3–arginine interaction in the inhibitors described here.

A comparison of the Compound-1/caspase-3 and Compound-9/caspase-8 structures demonstrates that substitutions at the N1 urazole are capable of following different trajectories to access the S_4 pocket. Both inhibitors place aromatic groups within this pocket, with the phenyl moiety of Compound-1 deeper in the pocket, and the azaindole of Compound-9 extending further along the peptide-binding groove. The positions of the oxygen atoms of the amides linking the aromatic groups to the urazole rings in the two compounds, however, differ by 3.8 Å. The orientation of the linker in Compound-1, in particular, suggests the feasibility of appending a group from the C4 position that might also access the S_4 pocket.

The shallow depression that is the S_2 subsite in both caspase-3 and caspase-8 imparts selectivity for substrates with small hydrophobic P_2 groups. This subsite is partially occupied by the C4, C5 and C6 atoms of the urazolopyridazine core. The saturated carbocyclic fusion of R2 to R3 utilized in some inhibitors, e.g., Compound-1 and Compound-6 (Fig. 6), presents a good opportunity to extend the inhibitors past this pocket and provides opportunities for further elaboration. The cyclohexyl moiety of Compound-9 extends even further from the bicyclic core, and approaches the S_1' subsite. Trying to directly engage the S_1' subsite using structure based drug design with the series of inhibitors described here presents an interesting challenge because it is reasonable to assume that this subsite overlaps the binding site of the dichlorobenzoic acid leaving group that is displaced during the course of the reaction.

4.4. Inhibitor binding at a secondary pocket in caspase-8

Hardy et al. [64] have proposed the existence of allosteric sites in caspases. These sites were initially identified while screening caspase-3 against a collection of thiol containing compounds. Subsequent analysis, and the determination of cocrystal structures with caspase-7 revealed a binding site close to the heterodimer–heterodimer interface, 14 Å from the active site. Mutagenesis experiments, and the synthesis of thiol-free analogs, both demonstrated that the formation of a cysteine:ligand covalent bond in the allosteric pocket is required for inhibition by this class of compounds [64]. Further mutational, kinetic, and structural studies in caspase-1 suggested that it contains an allosteric circuit of residues connecting two active sites [65]. Recent studies in caspase-7 have highlighted the role of this allosteric switch in the transition from its inactive, zymogen state to its proteolytically active form [66]. The shapes and precise locations of concave pockets at heterodimer–heterodimer interfaces are not conserved across different caspases [66]. Indeed, DTT, which is bound in one such pocket in caspase-8 [38] (and described above) does not appear to bind to caspase-3.

Our observation that Compound-4 has a secondary binding site on caspase-8 demonstrates that it is possible to target a drug-like, non-covalent small molecule to the proposed allosteric pockets of caspases (Fig. 9). The volume of the concave pocket occupied by Compound-4 is small: modeling shows that it is of an appropriate size, shape, and hydrophobicity to accommodate a single phenylalanyl or tyrosyl residue. The affinity of Compound-4 for this site would therefore be expected to be comparatively weak. Exploiting the proximal two-fold symmetry axis (Fig. 9) may provide an approach to enhancing the potency of compounds containing chlorophenyl acetic acid amide or similar moieties. Joining two such moieties with an appropriate linker could provide an advantage through avidity. Because the residues which form the binding pocket are not conserved across caspases, it is likely that such inhibitors would be caspase-specific.

In conclusion, this study examines a novel urazolopyridazine template for caspase inhibition that mimics the β-strand structure of substrates for these enzymes. These compounds are potent and fairly selective inhibitors of caspase-3 and caspase-8, and we provide herein a detailed kinetic analysis of enzyme inhibition and high-resolution X-ray crystallographic structures of three enzyme/inhibitor complexes. Interest in the caspases as therapeutic targets in a number of diseases where apoptosis plays a defining role is fueled by the obvious link between caspase action and cell death. Biologically, the picture is

complicated by the existence of over a dozen potential caspase targets that are similar in mechanism and substrate recognition.

There is still much to be learned about the precise roles and interrelationships of individual caspases in cellular dysfunction, and selective inhibition of any one caspase may prove to be a daunting task. The more we can learn about the detailed interactions between caspases and their substrates or inhibitors, the closer we come to being able to design specific drugs for specific diseases. The class of caspase inhibitors described in the present work expands our view of the catalytic sites in both an initiator and an executioner caspase. Hopefully, these findings will provide insights as to the design of drugs for multiple therapeutic indications that intervene at specific points in the apoptotic cascade.

Acknowledgments

We thank Thomas L. Emmons for helpful discussions, and also the staff of the IMCA-CAT beamlines. Use of the IMCA-CAT beamline 17-ID at the Advanced Photon Source was supported by the companies of the Industrial Macromolecular Crystallography Association through a contract with the Illinois Institute of Technology. Use of the Advanced Photon Source was supported by the US Department of Energy, Office of Science, Office of Basic Energy Sciences, under contract no. W-31-109-Eng-38.

References

[1] S. Elmore, Apoptosis: a review of programmed cell death, Toxicol. Pathol. 35 (2007) 495–516.
[2] P. Meier, A. Finch, G. Evan, Apoptosis in development, Nature 407 (1997) 796–801.
[3] N.N. Danial, S.J. Korsmeyer, Cell death: critical control points, Cell 116 (2004) 205–219.
[4] R.M. Siegel, Caspases at the crossroads of immune-cell life and death, Nat. Rev. Immunol. 6 (2006) 308–317.
[5] J.F. Kerr, C.M. Winterford, B.V. Harmon, Apoptosis: its significance in cancer and cancer therapy, Cancer 73 (1994) 2013–2026.
[6] A. Worth, A.J. Thrasher, H.B. Gaspar, Autoimmune lymphoproliferative syndrome: molecular basis of disease and clinical phenotype, Br. J. Hematol. 133 (2006) 124–140.
[7] A. Benchoua, C. Guégan, C. Couriaud, H. Hosseini, N. Sampaïo, D. Morin, B. Onténiente, Specific caspase pathways are activated in the two stages of cerebral infarction, J. Neurosci. 21 (2001) 7127–7134.
[8] J. Yuan, B.A. Yanker, Apoptosis in the nervous system, Nature 407 (2000) 802–809.
[9] G. Tezel, M. Wax, Inhibition of caspase activity in retinal cell apoptosis induced by various stimuli in vitro, Invest. Ophthalmol. Vis. Sci. 40 (1999) 2660–2667.
[10] J. Narula, P. Panday, E. Arbstini, N. Haider, N. Narula, F.D. Kolodgie, B. Dal Bello, M.J. Semigran, A. Bielsa-Masdeu, G.W. Dec, S. Israels, M. Ballester, R. Virmani, S. Saxena, S. Kharbanda, Apoptosis in heart failure: release of cytochrome *c* from mitochondria and activation of caspase-3 in human cardiomyopathy, Proc. Natl Acad. Sci. USA 96 (1999) 8144–8149.
[11] T.L. Vanden, Y. Qin, K. Wojcik, C.Q. Li, Z.H. Shao, T. Anderson, L.B. Becker, K.J. Hamann, Reperfusion and not simulated ischemia initiates apoptosis injury in chick cardiomyocytes, Am. J. Physiol. Heart Circ. Physiol. 284 (2003) H141–H150.
[12] R.S. Hotchkiss, D.W. Nicholson, Apoptosis and caspases regulate death and inflammation in sepsis, Nat. Rev. Immunol. 6 (2006) 813–822.
[13] H.A. Kim, F.J. Blanco, Cell death and apoptosis in osteartritic cartilage, Curr. Drug Targets 8 (2007) 333–345.
[14] C.A. Dinarello, Therapeutic strategies to reduce IL-1 activity in treating local and systemic inflammation, Curr. Opin. Pharmacol. 4 (2004) 378–385.
[15] S. Nakae, Y. Komiyama, H. Yokoyama, A. Nambu, M. Umeda, M. Iwase, I. Homma, K. Sudo, R. Horai, M. Asano, Y. Iwakura, IL-1 is required for allergen-specific Th_2 cell activation and the development of airway hypersensitivity response, Int. Immunol. 15 (2003) 483–490.
[16] K. Takeda, J. Stagg, H. Yagita, K. Okumura, M.J. Smyth, Targeting death-inducing receptors in cancer therapy, Oncogene 26 (2007) 3745–3757.
[17] S. Cornelius, K. Kersse, N. Festjens, M. Lamkanfi, P. Vandenabeele, Inflammatory caspases: targets for novel therapies, Curr. Pharm. Des. 13 (2007) 367–385.
[18] S.D. Linton, Caspase inhibitors: a pharmaceutical industry perspective, Curr. Top. Med. Chem. 5 (2005) 1697–1717.
[19] T. O'Brien, D. Lee, Prospects for caspase inhibitors, Mini-Rev. Med. Chem. 4 (2004) 153–165.
[20] N.A. Thornberry, Y. Lazebnik, Caspases: enemies within, Science 281 (1998) 1312–1316.
[21] M.O. Hengartner, The biochemistry of apoptosis, Nature 407 (2000) 770–776.
[22] S.J. Riedl, Y. Shi, Molecular mechanism of cell regulation during apoptosis, Nat. Rev. Mol. Cell Biol. 5 (2004) 897–907.
[23] S. Kumar, Caspase function in programmed cell death, Cell Death Differ. 14 (2007) 32–43.
[24] S.K. Rupinder, A.K. Gurpreet, S. Manjeet, Cell suicide and caspases, Vascul. Pharmacol. 46 (2007) 383–393.
[25] D.W. Chang, D. Ditsworth, H. Liu, S.M. Srinivasula, E.S. Alnemri, X. Yang, Oligomerization is a general mechanism for the activation of apoptosis initiator and inflammatory procaspases, J. Biol. Chem. 278 (2003) 16466–16469.
[26] P. Fuentes-Prior, G.S. Salvesen, The protein structure that shapes caspases activity, specificity, activation and inhibition, Biochem. J. 384 (2004) 201–232.
[27] S.J. Riedl, G.S. Salvesen, The apoptosome: signaling platform of cell death, Nat. Rev. Mol. Cell Biol. 8 (2007) 405–413.
[28] N.P.C. Walker, R.V. Talanian, K.D. Brady, L.C. Dang, N.J. Bump, C.R. Ferenz, S. Franklin, T. Ghayur, M.C. Hackett, L.D. Hammill, L. Herzog, M. Hugunin, W. Houy, J.A. Mankovich, L. McGuiness, E. Orlewicz, M. Paskind, C.A. Pratt, P. Reis, A. Summani, M. Terranova, J.P. Welch, L. Xiong, A. Möller, D.E. Tracey, R. Kamen, W.W. Wong, Crystal structure of the cysteine protease interleukin-1β-converting enzyme: a $(p20/p10)_2$ homodimer, Cell 78 (1994) 343–352.
[29] K.P. Wilson, J. Black, J.A. Thomson, E.E. Kim, J.P. Griffith, M.A. Navia, M.A. Murcko, S.P. Chambers, R.A. Aldape, S.A. Raybuck, S.J. Livingston, Structure and mechanism of interleukin-1β converting enzyme, Nature 370 (1994) 270–275.
[30] A. Schweizer, C. Briand, M.G. Gruetter, Crystal structure of caspase-2, apical initiator of the intrinsic apoptotic pathway, J. Biol. Chem. 278 (2003) 42441–42447.
[31] J. Rotonda, D.W. Nicholson, K.M. Fazil, M. Gallant, Y. Gareau, M. Labelle, E.P. Peterson, D.M. Rasper, R. Ruel, J.P. Vaillancourt, N.A. Thornberry, J.W. Becker, The three dimensional structure of apopain/CPP32, a key mediator of apoptosis, Nat. Struct. Biol. 3 (1996) 619–625.
[32] P.R. Mittl, S. Di Marco, J.F. Krebs, X. Bai, D.S. Karanewsky, J.P. Priestle, M.G. Grütter, Structure of recombinant human CPP32 in complex with the tetrapeptide acetyl-Asp-Val-Ala-Asp fluoromethyl ketone, J. Biol. Chem. 272 (1997) 6539–6547.
[33] D. Lee, S.A. Long, J.L. Adamsa, G. Chanc, K.S. Vaidyac, T.A. Francisc, K. Kiklyd, J.D. Winklere, C.-M. Sunge, C. Debouckf, S. Richardsonf, M.A. Levyg, W.E. DeWolf Jr., P. M. Kellerg, T. Tomaszekg, M.S. Headh, M.D. Ryanh, R.C. Haltiwangerh, P.-H. Liangi, C.A. Jansoni, P.J. McDevitti, K. Johansoni, N.O. Conchaj, W. Chanj, S.S. Abdel-Meguidj, A.M. Badgerk, M.W. Larkk, D.P. Nadeauk, L.J. Suvak, M. Gowenk, M.E. Nuttallkl, Potent and selective nonpeptide inhibitors of caspases 3 and 7 inhibit apoptosis and maintain cell functionality, J. Biol. Chem. 275 (2000) 16007–16014.
[34] R. Ganesan, P.R.E. Mittl, S. Jelakovic, M.G. Gruetter, Extended substrate recognition in caspase-3 revealed by high resolution X-ray structure analysis, J. Mol. Biol. 359 (2006) 1378–1388.
[35] R. Baumgartner, G. Meder, C. Briand, A. Decock, A. D'Arcy, U. Hassiepen, R. Morse, M. Renatus, The crystal structure of caspase-6, a selective effector of axonal degeneration, Biochem. J. 423 (2009) 429–439.
[36] J. Chai, Q. Wu, E. Shiozaki, S.M. Srinivasula, E.S. Alnemri, Y. Shi, Crystal structure of procaspase-7 zymogen: mechanism of activation and substrate binding, Cell 107 (2001) 399–407.
[37] S.J. Riedl, P. Fuentes-Prior, M. Renatus, N. Kairies, S. Krapp, R. Huber, G.S. Salvesen, W. Bode, Structural basis for the activation of human procaspase-7, Proc. Natl Acad. Sci. USA 98 (2001) 14790–14795.
[38] W. Watt, K.A. Koeplinger, A.M. Mildner, R.L. Heinrikson, A.G. Tomasselli, K.D. Watenpaugh, The atomic resolution structure of caspase-8, a key activator of apoptosis, Structure 7 (1999) 1135–1143.
[39] H. Blanchard, L. Kodandapani, P.R.E. Mittl, S. Di Marco, J.K. Krebs, J.C. Wu, K.J. Tomaselli, M.G. Grütter, The three dimensional structure of caspase-8: an initiator enzyme in apoptosis, Structure 7 (1999) 1125–1133.
[40] H. Blanchard, M. Donepudi, M. Tschopp, L. Kodandapani, J.C. Wu, M.G. Grutter, Caspase -8 specificity probed at subsite S4: crystal structure of the caspase-8–Z-DEVD-cho complex, J. Mol. Biol. 302 (2000) 9–16.
[41] M. Renatus, H.R. Stennicke, F.L. Scott, R.C. Liddington, G.S. Salvesen, Dimer formation drives the activation of the cell death protease caspase-9, Proc. Natl Acad. Sci. USA 98 (2001) 14250–14255.
[42] A.S. Ripka, D.H. Rich, Peptidomimetic design, Curr. Opin. Chem. Biol. 2 (1998) 441–452.
[43] A. Albeck, S. Kliper, Mechanism of cysteine protease inactivation by peptidyl epoxides, Biochem. J. 322 (1997) 879–884.
[44] D. Bromme, J.L. Klaus, K. Okamoto, D. Rasnick, J.T. Palmer, Peptidyl vinyl sulphones: a new class of potent and selective cysteine protease inhibitors-S2P2 specificity of human cathepsin O2 in comparison with cathepsins S and L, Biochem. J. 315 (1996) 85–89.
[45] H.-O. Kim, M. Kahn, A merger of rational drug design and combinatorial chemistry: development and application of peptide secondary structure mimetics, Comb. Chem. High Throughput Screen. 3 (2000) 167–183.
[46] P.D. Boatman, C.O. Ogbu, M. Eguchi, H.-O. Kim, H. Nakanishi, B. Cao, J.P. Shea, M. Kahn, Secondary structure peptide mimetics: design, synthesis, and evaluation of β-strand mimetic thrombin inhibitors, J. Med. Chem. 42 (1999) 1367–1375.
[47] R. St. Charles, J.H. Matthews, E. Zhang, A. Tulinsky, Bound structures of novel P_3–P'_1 β-strand mimetic inhibitors of thrombin, J. Med. Chem. 42 (1999) 1376–1383.
[48] K.B. Rank, A.N. Mildner, W.J. Leone, K.A. Koeplinger, K.C. Chou, A.G. Tomasselli, R.L. Heinrikson, S.K. Sharma, [W206R]-Procaspase-3; an inactivatable substrate for caspase-8, Protein Expr. Purif. 22 (2001) 258–266.
[49] K.A. Koeplinger, A.M. Mildner, J.W. Leone, J.S. Wheeler, R.L. Heinrikson, A.G. Tomasselli, Caspase-8: an efficient method for autoactivation of recombinant procaspase-8 by matrix absorption and characterization of the active enzyme, Protein Expr. Purif. 18 (2000) 378–387.

[50] T. Little, J. Meara, F. Ruan, M. Nguyen, M. Qabar, Efficient synthesis of novel 4-substituted urazoles, Synthetic Communications 32 (2002) 1741–1749.
[51] P.D. Boatman, J. Urban, M. Nguyen, M. Qabar, M. Kahn, High-throughput synthesis and optimization of thrombin inhibitors via urazole α-addition and Michael addition, Bioorg. & Med. Chem. Lett. 13 (2003) 1445–1449.
[52] Z. Otwinowski, W. Minor, Processing of X-ray diffraction data collected in oscillation mode, Meth. Enzymol. 276 (1997) 307–326.
[53] Collaborative Computational Project No. 4, The CCP4 suite: programs for protein crystallography, Acta Crystallogr., Sect D: Biol. Crystallogr 50 (1994) 760–763.
[54] J. Nazava, AMoRe: An automated package for molecular replacement, Acta Crystallogr. A50 (1994) 157–163.
[55] Bruker Analytical X-ray Systems, SHELXTL Software Reference Manual, Bruker Analytical X-ray Systems, Madison, WI, USA, 1997.
[56] G.N. Murshudov, A.A. Vagin, E.J. Dodson, Refinement of macromolecular structures by maximum-likelihood method, Acta Crystallogr. D Biol. Crystallogr. 53 (1997) 240–255.
[57] J.S. Sack, F.A. Quiocho, CHAIN Crystallographic Modeling Program, Baylor College of Medicine, Houston, TX, USA, 1992.
[58] B.C. Finzel, Mastering the LORE of protein structure, Acta Crystallogr. D Biol. Crystallogr. 51 (1995) 450–457.
[59] P. Emsley, K. Cowtan, Coot: model-building tools for molecular graphics, Acta Cryst. D60 (2004) 2126–2132.
[60] R.A. Laskowski, M.W. MacArthur, D.S. Moss, J.M. Thornton, PROCHECK: a program to check the stereochemical quality of protein structures, J. Appl. Crystallogr. 26 (1993) 283–291.
[61] P. Kuzmic, Program DYNAFIT for the analysis of enzyme kinetic data: application to HIV proteinase, Anal. Biochem. 237 (1996) 260–273.
[62] R. Ganesan, P.R.E. Mittl, S. Jelkovic, M.G. Grutter, Extended substrate recognition in caspase-3 revealed by high resolution X-ray analysis, J. Mol. Biol. 359 (2006) 1378–1388.
[63] N.A. Thornberry, T.A. Rano, E.P. Peterson, D.M. Rasper, T. Timkey, M. Garcia-Calvo, V.M. Houtzager, P.A. Nordstrom, S. Roy, J.P. Vaillancourt, K.T. Chapman, D.W. Nicholson, A combinatorial approach defines specificities of members of the caspase family and granzyme B, J. Biol. Chem 272 (1997) 17907–17911.
[64] J.A. Hardy, J. Lam, T. O'Brien, J.A. Wells, Discovery of an allosteric site in the caspases, Proc. Natl Acad. Sci. USA 101 (2004) 12461–12466.
[65] D. Datta, J.M. Scheer, M.J. Romanowski, J.A. Wells, An allosteric circuit in caspase-1, J. Mol. Biol. 381 (2008) 1157–1167.
[66] J.A. Hardy, J.A. Wells, Dissecting an allosteric switch in caspase-7 using chemical and mutational probes, J. Biol. Chem. 284 (2009) 26063–26069.